Received: 10 February 2023 | Revised: 5 April 2023 | Accepted: 6 April 2023

DOI: 10.1002/pmic.202300082

Proteomics
Proteomics and Systems Biology

RESEARCH ARTICLE

Charge site manipulation to enhance top-down fragmentation efficiency

Tanja Habeck | **Edvaldo Vasconcelos Soares Maciel** | **Kevin Kretschmer** | **Frederik Lermyte**

Department of Chemistry, Clemens-Schöpf-Institute of Chemistry and Biochemistry, Technical University of Darmstadt, Darmstadt, Hessen, Germany

Correspondence
Frederik Lermyte, Department of Chemistry, Clemens-Schöpf-Institute of Chemistry and Biochemistry, Technical University of Darmstadt, 64287 Darmstadt.
Email: frederik.lermyte@tu-darmstadt.de

Funding information
Fonds der Chemischen Industrie, Grant/Award Number: 661715; Alexander von Humboldt-Stiftung, Grant/Award Number: Humboldt-Forschungsstipendium für Postdocs; Hessisches Ministerium für Wissenschaft und Kunst, Grant/Award Number: LOEWE Schwerpunkt TRABITA; Deutsche Forschungsgemeinschaft, Grant/Award Number: 461372424; Technische Universität Darmstadt, Grant/Award Number: Career Bridging Grant

Abstract

In recent years, top-down mass spectrometry has become a widely used approach to study proteoforms; however, improving sequence coverage remains an important goal. Here, two different proteins, α-synuclein and bovine carbonic anhydrase, were subjected to top-down collision-induced dissociation (CID) after electrospray ionisation. Two high-boiling solvents, DMSO and propylene carbonate, were added to the protein solution in low concentration (2%) and the effects on the top-down fragmentation patterns of the proteins were systematically investigated. Each sample was measured in triplicate, which revealed highly reproducible differences in the top-down CID fragmentation patterns in the presence of a solution additive, even if the same precursor charge state was isolated in the quadrupole of the instrument. Further investigation supports the solution condition-dependent selective formation of different protonation site isomers as the underlying cause of these differences. Higher sequence coverage was often observed in the presence of additives, and the benefits of this approach became even more evident when datasets from different solution conditions were combined, as increases up to 35% in cleavage coverage were obtained. Overall, this approach therefore represents a promising opportunity to increase top-down fragmentation efficiency.

KEYWORDS
electrospray ionization mass spectrometry (ESI-MS), mass spectrometry, top-down proteomics

1 | INTRODUCTION

Analysing intact proteins with tandem mass spectrometry (MS), an approach known as top-down analysis, is a powerful tool to map post-translational modifications and analyse protein sequences. In contrast to bottom-up, top-down MS is the only method able to assign all modifications that are present to their associated amino acid residues [1–7].

Increasing fragmentation efficiency is a key goal in top-down MS to gain more detailed sequence information. In the most common ionisation method, electrospray ionisation (ESI), more than one charge state of the protein analyte is observed [8]. Multiple charges lead to reduced *m/z* values, which allows detection of intact proteins with a range of instruments [9]. Additionally, the charge state

Abbreviations: αSN, alpha-synuclein; AmAc, ammonium acetate; CA, carbonic anhydrase; ETD, electron transfer dissociation; FAIMS, high-field asymmetric waveform ion mobility spectrometry; IM, ion mobility; IMS, ion mobility spectrometry; IRMPD, infrared multiphoton dissociation; *m/z*, mass/charge; PC, propylene carbonate; UVPD, ultraviolet photodissociation.

distribution can be altered by addition of so-called supercharging or charge-modifying agents. In general, higher charge states enhance the fragmentation efficiency, and supercharging can be used to obtain more backbone fragmentation [10–15]. Additionally, charge modifiers have been used to increase sensitivity in top-down LC-MS applications [16].

Another way of using solvent additives involves altering charge sites rather than the overall charge state. This leads to the formation of protonation isomers (so called 'protomers') which have been extensively described in the small-molecule literature. Ion mobility spectrometry (IMS), gas-phase spectroscopy and selective photodissociation have been the most common techniques in these studies [17–29]. IMS has been shown capable of separating protomers of surfactin, a cyclic peptide larger than 1 kDa [30]. In contrast to small molecules and peptides, the formation of distinct protomers of intact protein ions has not been extensively studied. In one recent example, Zhang et al. observed different protomers in high charge states of denatured intact carbonic anhydrase (CA), and separated them with high-field asymmetric waveform ion mobility spectrometry (FAIMS). Additionally, different fragmentation behaviour was observed for the different protomers [31]. Around the same time, the first report was published of the selective formation and identification of specific protomers of intact protein ions by the addition of 10% DMSO to the protein solution [32].

There are several factors that determine gas-phase protein protonation sites. Gas- and solution-phase basicities are different, and Coulombic repulsion—which depends to some extent on protein conformation—can also affect how favourable certain sites are. Protons do not always rearrange to the gas-phase optimal sites during the ESI process, and different solvent properties—including dielectric permittivity and proticity—can play a role. Several mechanisms of charging and supercharging of proteins in ESI have been proposed in the literature, and extensive supercharging is associated with extended, near-linear conformations [33–37].

The link between proton locations, net charge state and preferred cleavage sites in 'slow heating' dissociation methods such as CID can be understood through the 'mobile-proton model' developed mainly by Wysocki and Gaskell [38–41]. Although protons are significantly mobilised at high internal energies in this model, their starting location does affect the preference between different fragmentation pathways. Several models have been developed to determine favoured charge sites and their influence on fragmentation, and experiments with model proteins have been performed to support these models [42–45].

Based on the above, we hypothesised that altering the ESI conditions could be used to induce the formation of a greater protomer variety of intact proteins without changing the overall charge state, and that this would lead to a greater variety of fragments, potentially making this approach a useful tool for top-down protein analysis. We chose propylene carbonate (PC) and DMSO, as both are commonly used ESI additives with comparable physicochemical properties, which allowed us to link protomer formation to specific properties of the ESI solvent. With their high boiling point and low dielectric constant compared to water, these aprotic additives are enriched in the ESI droplet and consequently even low amounts allow charge site manipulation without having a significant impact on the protein in bulk solution.

Significance of the study

This work uses different mass spectrometry methods to demonstrate a new systematic approach to modify charge sites in intact protein ions using solvent additives. Even small amounts of these additives can be used to manipulate protonation positions and thus alter the top-down fragmentation behaviour of proteins in collision-induced dissociation. This is advantageous as it leads to a greater variety of fragments, which can be used for improved characterisation of potentially unknown proteoforms. The approach developed here provides the opportunity to use the widely available collision-induced dissociation method for more efficient top-down protein fragmentation. As such, it represents a method to obtain a more informative top-down mass spectrometry experiment for current practitioners, as well as make effective top-down protein analysis accessible to more researchers.

In earlier work, the intrinsically disordered protein alpha-synuclein was sprayed from both purely aqueous solution and with the addition of 10% DMSO. It was shown that this addition altered the CID fragmentation of αSN^{14+}, and UVPD revealed differences in proton locations [32]. In the current study, we have extended the above investigation by using two charge modifying agents (PC and DMSO). We also significantly reduced the concentration of these additives (from 10% to 2%) compared to the previous work to minimise any effect on the protein in bulk solution. Additionally, the work was extended to a second charge state (10+) of alpha-synuclein, and to a second protein (carbonic anhydrase) to investigate whether this phenomenon has the potential to be widely applicable.

2 | MATERIALS AND METHODS

Human α-synuclein (αSN) and bovine carbonic anhydrase (CA) were used for the experiments. A 5 μM solution of αSN was prepared in 20 mM ammonium acetate (AmAc) in water. A 10 μM solution of CA was prepared in 30:70 water:methanol (MeOH) and 1% formic acid (FA). The respective additives, propylene carbonate and DMSO, were added to the protein solution in a concentration of 2% (v/v). Important physicochemical properties of solvents and additives used in this work are summarised in Table S1. These solutions were prepared independently three times for each condition so that triplicate measurements could be performed.

All protein solutions were sprayed via direct infusion with a nanoESI setup and in-house pulled glass needles coupled to a Waters Synapt

XS ion mobility—mass spectrometer. The needles were pulled with a Sutter P97 needle puller. For all samples a capillary voltage of 0.8–1.5 kV was used. For αSN the sampling cone was set to 10 V, and for CA to 100 V. Source offset values were set to 1 V for all samples. The other settings were kept at their default values. Ion mobility measurements were performed with an IMS wave height of 40 V and three different wave velocities (700, 900, and 1100 m/s) and calibrated with denatured myoglobin. A logarithmic fit was applied to calculate collision cross-section (CCS) values [46, 47].

Top-down CID was carried out in the Trap cell. Precursor charge states were selected in the quadrupole and CA^{32+} was fragmented with 25 V, αSN^{10+} with 45 V, and αSN^{14+} with 20 V of collision energy. All experiments were performed in triplicate, and all spectra were acquired for 10 min. Fragment ion analysis was done using MASHNative with eTHRASH deconvolution [48–52]. Fragments were automatically assigned with a filter of <10 ppm mass error and were additionally validated manually. Intensities were extracted from MASH and normalised to the TIC to ensure comparability between different samples. Only fragments which were consistently detected in all three replicates were considered for further evaluation. To look at specific cleavage positions, the average intensities of all fragment types which resulted from a bond cleavage at this specific residue position were summed up. Standard deviations for each specific fragment intensity were calculated based on the triplicate measurements, and the shown standard deviations for their ratios were calculated with error propagation. As they spanned several orders of magnitude, the ratios were log-transformed before plotting, and the standard deviations are shown as relative values as a result. Relative intensities for selected fragment sites are provided in Table S2.

For ETD fragmentation, 1,4-dicyanobenzene was used as a radical anion. For all experiments a glow discharge current of 80 μA and a make-up gas flow of 50 mL/min was used. For the CA samples, a capillary voltage of 1.8 to 2 kV was applied using 50 V of cone voltage. For αSN, 1 to 1.5 kV of capillary voltage and cone voltage of 10 V were used. A Trap gas flow of either 11 mL/min (αSN) or 15 mL/min (CA) and a Transfer gas flow of 0.9 mL/min were used. The Trap wave height was set to 0.3 to 0.4 V to achieve sufficient fragmentation. ETD fragment assignment was performed manually.

3 | RESULTS AND DISCUSSION

3.1 | 14+ alpha-synuclein

3.1.1 | Top-down CID reveals differences in fragmentation pattern

To test our hypothesis that we can manipulate specific protomer formation with low amounts of additives without influencing the conformation of the protein, we investigated the overall charge state distribution of the sprayed proteins, as well as the CCS values of the specific charge states. The overall charge state distribution can give a first indication of protein conformation, with unfolded states being associated with higher charge states and a broad charge state distribution [53, 54]. We investigated the influence of the low amount of charge modifier on the charge state distribution of αSN (Figure S1A). Addition of 2% PC or DMSO slightly shifted the intensity-weighted average charge state to a lower number, from (10.6 ± 0.1) to (9.7 ± 0.2) and (9.4 ± 0.2), respectively (standard deviation calculated from triplicate measurements). This change of around 10% indicated only a small effect and in both cases no supercharging of αSN was observed. Additionally, we performed ion mobility measurements, and the resulting CCS values (see Figure S2) showed no significant change for either αSN^{10+} or αSN^{14+}.

All top-down CID experiments were carried out in triplicate, with independently prepared samples, and fragments were only considered for our analysis if they were consistently present in all three measurements. Interestingly, and in agreement with previous work [32], a distinct fragmentation pattern (shown in Figure 1) for each solution condition was observed. Each dot represents an observed fragment at the respective cleavage site. The stated coverage is calculated as the number of observed cleavage sites divided by the number of all inter-residue bonds. Specific regions seemed to fragment more efficiently when PC or DMSO was added, that is, those around residues Val71 and Gly111. Even if the overall coverage was not always significantly increased when adding the charge modifier, complementary fragments were often formed and it proved especially beneficial to combine two datasets (one without, and one with additive; see yellow and orange dots in the upper part of Figure 1). This approach led to an increase in coverage from 18% to 25% for individual datasets, to nearly 30% for the combinations, which represents a relative increase of around 30%. Because we only considered fragments that were consistently present, this effect cannot be due to random experimental fluctuations, but instead must be due to the different solution conditions.

3.1.2 | Change in specific cleavage site intensities

In addition to the same fragments usually being observed across replicate top-down CID experiments, the relative fragment intensities (i.e., normalised to the total ion current) also showed a high reproducibility for samples with as well as without additives, and overall standard deviations were relatively low. As proteoform characterisation, rather than quantitation, has been the focus of most top-down proteomics studies, this high degree of reproducibility is perhaps underappreciated and to some extent even unexpected in the MS community. It should be mentioned that quantitative top-down approaches are often based on MS1-level data and use liquid chromatography separation. As such, our experiments allowed averaging of a higher number of spectra than what is typical [55–57]. The general point on reproducible fragment ion intensity is still worth noting, however, and might in future allow the inclusion of specific fragmentation efficiency in the toolbox of quantitative methods.

Furthermore, while normalised fragment intensities were quite reproducible for replicate measurements performed under the same

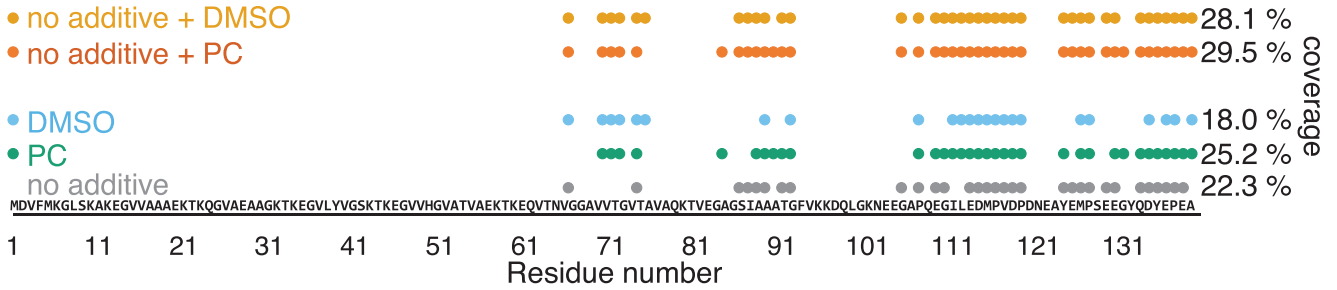

FIGURE 1 Top-down CID fragmentation pattern of αSN^{14+}. Cleavage sites consistently observed in all three independent measurements for each condition are plotted as dots. Residue number and the sequence of αSN are shown on the horizontal axis. From bottom to top, the cleavage sites from the different samples (grey: no additive; green: PC; blue: DMSO) and the results from the combined datasets (orange: 'no additive' + 'PC' datasets; yellow: 'no additive' + 'DMSO') are shown. Cleavage coverage, calculated by dividing the number of observed cleavage sites by the number of inter-residue bonds of αSN, is indicated on the right side of the figure.

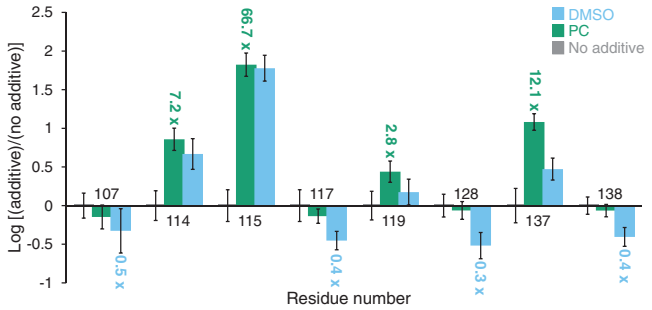

FIGURE 2 Changes in relative fragment intensities at specific cleavage sites of αSN^{14+} plotted as log-transformed values against residue numbers of the cleavage sites. The reference value (by definition zero after log-transformation) is shown in grey, results for the 'PC' dataset in green, and 'DMSO' data in blue (error bars indicate standard deviation). Negative values indicate a decrease of normalised fragment intensity compared to the additive-free reference value, whereas a positive value indicates an increase.

conditions, drastic differences at specific cleavage sites (see Figure 2) were observed when comparing solution conditions. As we were mostly interested in the change caused by a specific additive compared to the sample with no additive (referred to as the reference value) all normalised fragment intensities were divided by this reference value at the specific cleavage site. Note that the resulting ratios are log-transformed in Figure 2; therefore, by definition, the average value for the 'no additive' reference condition is zero.

The most significant changes in fragment intensities were observed in the C-terminal region of αSN, which is in line with the findings of an earlier publication where 10 % DMSO was added [32]. Additionally, the changes are consistent with the changes we observed in the fragmentation pattern in the region around residue Gly111 (vide supra). Especially, at residue Asp115 a substantially enhanced fragment intensity (up to 66-fold) was observed. Also worth emphasising is the comparable trend for both additives. This suggests that their similar properties as high-boiling and aprotic solvents are the drivers of this specific protomer formation, similar to earlier reports in the small-molecule literature [27].

3.1.3 | ETD supports the proposed selective protomer formation

Ideally, one would like to pinpoint the gas-phase protonation sites of a protein ion by tracking the charge state of all fragments, such that each protonation site would correspond to an increased charge state of fragments that contain that particular residue. Unfortunately, this is not possible with CID fragments because, as we have already mentioned, the mechanism involves mobilisation of protons, which makes an unambiguous statement about their initial position based on fragment charge states impossible [58–60]. Electron- and (high-energy) photon-based fragmentation methods, however, do not cause significant proton mobilisation and therefore do allow the correlation of fragment charge states and precursor charge sites. We subjected αSN^{14+} to ETD and compared the resulting *c*- and *z*-type ions from αSN sprayed with and without the addition of 2% PC. Figure 3 shows the resulting *c* (upper part) and *z* (lower part) fragments. The green triangles represent fragments observed with PC and the grey dots those without added modifiers. The detected fragments are plotted in rows that indicate their observed charge state(s). The protein sequence is also displayed in the figure, and the residues potentially carrying a charge based on the detected ETD fragments are highlighted. The orange-coloured ones show charge sites that are shared between both solvent conditions, whereas a green colour indicates protonation sites specific for PC, and sites unique to the additive-free sample are indicated in grey. In agreement with several other ETD and ECD studies of αSN, most fragments originated from cleavage near the N-terminus [61–64].

Looking at the ETD data in more detail, the region between Lys34 and Val55 is particularly interesting, as significant differences and unique charge sites between solution conditions were observed here. For *c*-type fragments of charge state 2+ and 3+, clear differences between the solution conditions are visible. c^{2+} ions were observed up to c_{33} for the additive-free sample, and only up to residue c_{24} in the presence of PC. Similarly, c^{3+} ions occurred up to c_{57} when the protein was sprayed from an additive-free sample, and only up to c_{38} when the sample contained 2% PC. If we focus on higher fragment charge states, a c^{6+} ion formed by cleavage at residue Lys34 was

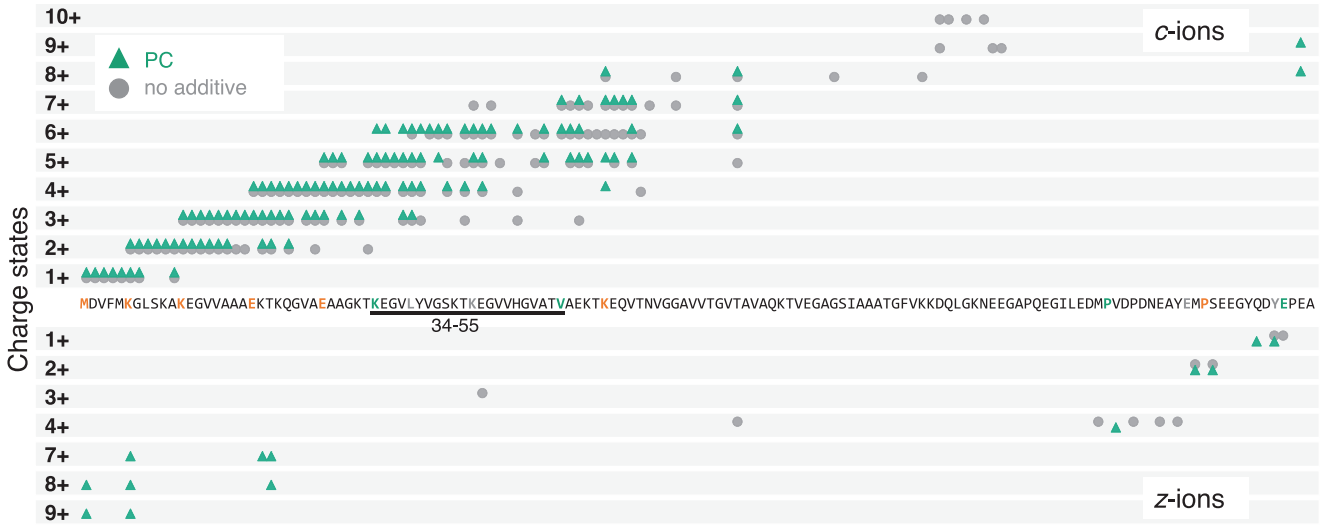

FIGURE 3 ETD fragmentation pattern of αSN^{14+} with and without 2% PC. The detected c (top) and z fragments (bottom) are shown, subdivided in rows that represent their charge states. Grey dots represent fragments from the no-additive sample and the green triangles fragments from the PC-containing sample. Residues highlighted in grey and green in the sequence (middle) represent charge sites unique to no-additive and PC-containing samples, respectively, and orange represents charge sites common to both samples. The [Lys34-Val55] region is highlighted as the largest number of differing charge sites was observed here.

observed in the spectrum of the PC-containing sample. Conversely, the first c^{6+} ion from the additive-free sample originated from cleavage at Leu38. Additionally, a number of highly charged (7–9+) large *z* ions (z_{119} to z_{140}) could be detected in ETD of αSN^{14+} sprayed from PC-containing solution, but not from the additive-free solution. All of the above is consistent with a shift of the ESI protonation sites toward the N-terminal region of αSN^{14+} in the presence of 2% PC. This finding is in line with the results of an earlier UVPD experiment that investigated charge sites of αSN^{14+} sprayed from a solution containing 10% DMSO [32]. To further investigate whether this selective protomer formation is limited to this specific charge state of αSN, we expanded our investigations to the 10+ charge state.

3.2 | 10+ alpha-synuclein

As already mentioned, the solution additives had no significant effect on the CCS value of αSN^{10+} (see Figure S2). Looking at the CID fragmentation pattern, where again triplicate measurements for each condition were performed, a similar trend was observed as for αSN^{14+}. As before, only fragments which were present in all three replicates are displayed in Figure 4A. In this case, both of the additive-containing samples (PC: green; DMSO: blue) showed a higher overall coverage, which became even more apparent when looking at the combined datasets (yellow and orange). An up to 35% increase in coverage (from *ca.* 55% to over 70%) was observed when comparing the combined datasets to the sample sprayed without an additive. For the 10+ charge state an overall higher number of cleavages was detected in comparison to the 14+ precursor. In part, this can be explained by the higher intensity of the 10+ precursor leading to better fragment signal intensity. However, given the very large increase in cleavage coverage upon adding PC or DMSO, as well as the higher coverage compared to the 14+ precursor even without additives, this case seems to provide a clear example of the benefit of manipulating charge sites rather than increasing the net charge state in order to maximise proteoform characterisation. As was observed for the 14+ precursor, the region around residue Gly111 again showed some of the clearest differences as a result of the change in solution conditions.

Figure 4B shows the site-specific changes in fragment intensity between different solution conditions, plotted in the same way as in Figure 2. Similar to our observations for the 14+ precursor, both additives follow the same trend; however, the magnitude of the changes is smaller. For the 14+ precursor, differences up to a 66-fold increase could be observed, whereas for the 10+ charge state, only changes up to 7.2-fold were observed. Additionally, the changes are more widely distributed over the whole sequence rather than being primarily located close to the C-terminus as for the 14+ precursor.

Looking at the ETD fragmentation pattern of αSN^{10+} (Figure 4C), the differences between different solution conditions are less clear compared to αSN^{14+}. This is mainly due to the lower overall coverage (around 26%–28% for the 10+, compared to 50%–60% for the 14+ precursor) as it is well known that ETD efficiency is strongly dependent on precursor charge state [65, 66]. However, the same overall shift of charge sites towards the N-terminus was apparent. In particular, when looking at the *z*-type fragments (bottom part of the figure), z_{130} to z_{140} fragments were detected with charge states ranging from 6+ to 9+ for the PC-containing sample and only one *z* fragment ($z_{140}{}^{8+}$) was present in ETD of αSN^{10+} sprayed from the additive-free sample. Another difference can be observed in the c^{4+} ion series. For the PC-containing sample, $c_{27}{}^{4+}$ was detected, whereas for the additive-free sample the smallest c^{4+} ion was $c_{34}{}^{4+}$. This further indicates that it was

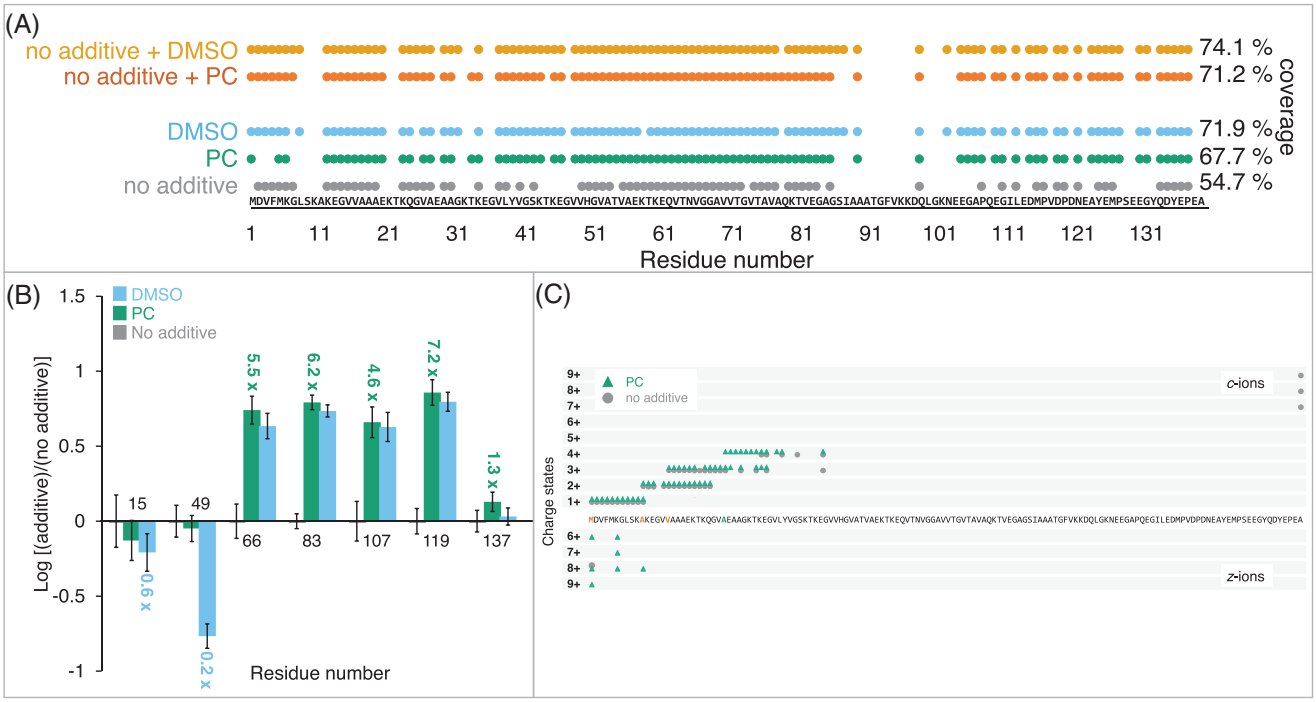

FIGURE 4 (A) Top-down CID fragmentation pattern of αSN^{10+} sprayed from different solutions. Cleavage sites consistently observed in all three independent measurements for each condition are plotted as dots. Cleavage sites from the different samples (grey: no additive; green: PC; blue: DMSO) and the results from the combined datasets (orange: 'no additive' + 'PC' datasets; yellow: 'no additive' + 'DMSO') are shown. Cleavage coverage is indicated on the right. (B) Solution condition-dependent changes in intensities at specific cleavage sites of αSN^{10+} plotted as log-transformed values against the residue numbers of the cleavage sites. The reference value (by definition zero after log-transformation) is shown in grey, 'PC' data in green, and 'DMSO' results in blue (error bars indicate standard deviation). (C) ETD fragmentation pattern of αSN^{10+} with and without 2% added PC. The detected c (top) and z fragments (bottom) are shown, subdivided in rows that represent their charge states. Grey dots represent fragments from the no-additive sample and green triangles from the PC-containing sample. Residues highlighted in grey and green in the sequence (middle) represent charge sites unique to no-additive and PC-containing samples, respectively, and orange represents charge sites common to both samples.

more likely that charges were shifted towards the N-terminus when the 10+ precursor was sprayed from a solution with 2% PC.

Having established that the formation of different protomers occurs in two different charge states of αSN, as well as having demonstrated the beneficial effect on cleavage coverage in CID, we next expanded our investigation to a different protein, carbonic anhydrase. As in our work with alpha-synuclein, we used both DMSO and PC as solvent additives.

3.3 | 32+ carbonic anhydrase

In contrast to the intrinsically disordered alpha-synuclein, carbonic anhydrase adopts a well-defined folded structure in aqueous solution. While the presence of 2% PC or DMSO is unlikely to significantly affect the native conformation in bulk solution, these additives are enriched in the electrospray droplet due to their high boiling point relative to water. As such, in-droplet unfolding would be a possible concern and could complicate comparison of samples with and without additives if spraying from native-like solution [37, 67]. To avoid this potential confounding effect, we sprayed from a denaturing solution (70% methanol, 1% formic acid) and focussed on the 32+ charge state of the protein. This state is largely unfolded and has little residual structure, which is further supported by the very small differences in charge state distributions and collision cross-sections between additive-containing and additive-free conditions (see Figures S1B and S3). As before, experiments were carried out in triplicate.

Figure 5A reveals differences in the top-down CID fragmentation pattern of CA^{32+} between the different solution conditions (grey: no additive; green: 2% PC; blue: 2% DMSO). Different regions distributed over the sequence were affected. The regions from residue Phe20 to Val60 and from Arg111 to Ala141 showed especially drastic differences in fragmentation pattern, which become even clearer when the datasets are combined. An increase of up to 20% in coverage (from just below 20% to nearly 24%) was achieved by combining datasets with and without charge modifiers. A closer investigation of fragment intensities from specific cleavage sites (see Figure 5B) further illustrates the impact of the solvent additive on CID fragmentation. The overall trend of affecting residue cleavage sites is comparable (albeit not as pronounced) as in the experiments with αSN. Site-specific fragment intensity increases of up to 3.1-fold, and decreases down to 0.7-fold were detected. The biggest intensity differences were observed in a region near the C-terminus (residues Leu184, Thr192, Leu197, Thr198 and Glu213).

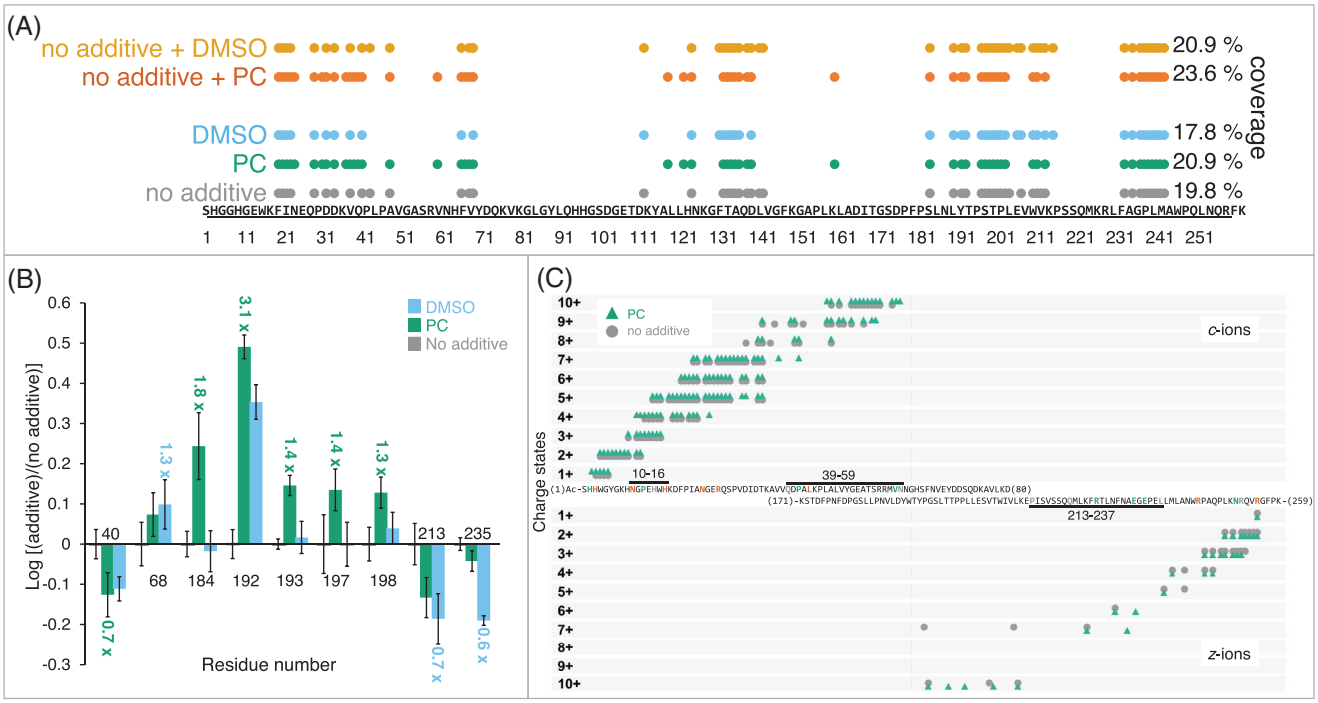

FIGURE 5 (A) Top-down CID fragmentation pattern of CA^{32+}. Cleavage sites consistently observed in all three independent measurements for each condition are plotted as dots. Residue number and sequence of CA are shown on the horizontal axis. Cleavage sites from the different samples (grey: no additive; green: PC; blue: DMSO) and the results from the combined datasets (orange: 'no additive' + 'PC' datasets; yellow: 'no additive' + 'DMSO') are shown. Cleavage coverage is indicated on the right. (B) Changes in intensities at specific cleavage sites of CA^{32+} plotted as log-transformed values against cleavage site residue numbers. The reference value (by definition zero after log-transformation) is shown in grey, 'PC' data in green, and 'DMSO' results in blue (error bars indicate standard deviation). (C) ETD fragmentation pattern of CA^{32+} with and without 2% added PC. The detected c (top) and z fragments (bottom) are subdivided in rows that represent their charge states. Grey dots represent fragments from the no-additive sample and the green triangles from the PC-containing sample. Residues highlighted in grey and green in the sequence (middle) represent charge sites unique to no-additive and PC-containing samples, respectively, and orange represents charge sites common to both samples. The regions from residue [Asn10-His16], [Val30-Val59] and [Pro213-Leu237] are highlighted as the largest number of differing charge sites were observed here.

The differences in cleavage site-specific intensities are also consistent with the work by Zhang et al., who suggested the existence of protomer families of CA^{32+} based on two species with identical CCS that could be separated with FAIMS. These authors observed intensity differences in CID of these protomer families, including of the fragments y_{67} and y_{25} [31]. These are formed by cleavage at Tyr193 and Glu235, where we also observed significant intensity differences (Figure 5B). In Figure 5C, ETD fragmentation differences are shown. Comparing c^{+}, c^{4+} and c^{10+} fragments showed a slight trend towards more charge sites in the N-terminal region of CA^{32+} in the sample with added PC. Conversely, for the additive-free sample, more protonation sites could be determined to be closer to the C-terminus when looking at z^{3+} and z^{5+} fragments. For the additive free-sample, ${z_9}^{3+}$ and ${z_{28}}^{5+}$ were detected; contrarily, for the PC-containing sample solution, only ${z_8}^{3+}$ and ${z_{23}}^{5+}$ were present.

4 | CONCLUDING REMARKS

As top-down protein mass spectrometry continues to become a more mainstream approach, there is an increasing need for methods to achieve extensive fragmentation of intact protein ions. Progress in electron- and photon-based methods in recent years has been remarkable; however, these require hardware modification to implement, and they also lead to the formation of different fragment types than collision-based methods, which can potentially complicate subsequent data analysis. In this work, we have extended earlier, preliminary experiments and demonstrated that the use of a low concentration of solvent additives can be used to cause selective formation of different protomers of intact protein ions. These have different cleavage site preferences and thus generate complementary (albeit partially overlapping) sets of fragments, and this effect can be used to boost sequence coverage in top-down MS. This makes a future implementation to liquid chromatography-based separations and consequently a higher-throughput application a desired goal, and work toward such an implementation is currently ongoing in our lab. Additionally, this approach requires no modifications to existing hardware or methods and generates the same fragment types that are typically observed in CID.

The two additives we tested share certain properties, specifically a higher boiling point and lower dielectric permittivity than water, as well as a lack of labile protons. While both additives usually caused a shift in fragment intensities in the same direction, the magnitude of the effect

often differed, which suggests that the aprotic nature of the additives is not the only relevant factor. Instead, variables such as permittivity (which could affect the preferred charge sites in solution) and boiling point (which affects the droplet evaporation rate and thus the time protons have to rearrange during the ESI process) might also play a role. The contributions of these factors will be explored in future work, as well as possible implications for our understanding of the mechanism of ESI under conventional conditions.

ACKNOWLEDGEMENTS

Financial support for this work was provided by LOEWE project TRABITA funded by the Hessian Ministry of Higher Education, Research, and the Arts (HMWK). The Synapt XS instrument was funded through a grant by the German Research Foundation (DFG), project number 461372424. E.V.S.M. was funded during the course of this work through a Career Bridging Grant from TU Darmstadt and a Humboldt Forschungsstipendium (Alexander von Humboldt Stiftung). Additional support by the Fonds der Chemischen Industrie is gratefully acknowledged. We are grateful to the reviewers for their valuable comments.

Open access funding enabled and organized by Projekt DEAL.

CONFLICT OF INTEREST STATEMENT

The authors declare no conflicts of interest.

DATA AVAILABILITY STATEMENT

The mass spectrometry proteomics data have been deposited to the ProteomeXchange Consortium via the PRIDE [68, 69] partner repository with the dataset identifier PXD039993.

ORCID

Tanja Habeck https://orcid.org/0000-0002-4325-6335
Edvaldo Vasconcelos Soares Maciel https://orcid.org/0000-0002-1231-7190
Frederik Lermyte https://orcid.org/0000-0001-7371-4475

REFERENCES

1. Smith, L. M., & Kelleher, N. L. (2013). Proteoform: A single term describing protein complexity. *Nature Methods*, *10*, 186–187.
2. Habeck, T., & Lermyte, F. (2023). Seeing the complete picture: Proteins in top-down mass spectrometry. *Essays in Biochemistry*, *67*, 283–300.
3. Cui, W., Rohrs, H. W., & Gross, M. L. (2011). Top-down mass spectrometry: Recent developments, applications and perspectives. *Analyst*, *136*, 3854–3864.
4. Loo, J. A., Edmonds, C. G., & Smith, R. D. (1990). Primary sequence information from intact proteins by electrospray ionization tandem mass spectrometry. *Science (New York, N.Y.)*, *248*, 201–204.
5. Kelleher, N. L., Lin, H. Y., Valaskovic, G. A., Aaserud, D. J., Fridriksson, E. K., & Mclafferty, F. W. (1999). Top down versus bottom up protein characterization by tandem high-resolution mass spectrometry. *Journal of the American Chemical Society*, *121*, 806–812.
6. Han, X., Jin, M., Breuker, K., & Mclafferty, F. W. (2006). Extending top-down mass spectrometry to proteins with masses greater than 200 kilodaltons. *Science (New York, N.Y.)*, *314*, 109–112.
7. Sze, S. K., Ge, Y., Oh, H., & McLafferty, F. W. (2002). Top-down mass spectrometry of a 29-kDa protein for characterization of any post-translational modification to within one residue. *Proceedings of the National Academy of Sciences USA*, *99*, 1774–1779.
8. Fenn, J. B., Mann, M., Meng, C. K., Wong, S. F., & Whitehouse, C. M. (1989). Electrospray ionization for mass spectrometry of large biomolecules. *Science (New York, N.Y.)*, *246*, 64–71.
9. Cech, N. B., & Enke, C. G. (2001). Practical implications of some recent studies in electrospray ionization fundamentals. *Mass Spectrometry Reviews*, *20*, 362–387.
10. Iavarone, A T., & Williams, E R. (2003). Collisionally activated dissociation of supercharged proteins formed by electrospray ionization. *Analytical Chemistry*, *75*, 4525–4533.
11. Zenaidee, M. A., & Donald, W. A. (2015). Electron capture dissociation of extremely supercharged protein ions formed by electrospray ionisation. *Analytical Methods*, *7*, 7132–7139.
12. Zhang, J., Loo, R. R. O, & Loo, J. A. (2015). Increasing fragmentation of disulfide-bonded proteins for top–down mass spectrometry by supercharging. *International Journal of Mass Spectrometry*, *377*, 546–556.
13. Wang, H., Yong, G., Brown, S. L., Lee, H. E., Zenaidee, M. A., Supuran, C. T., & Donald, W. A. (2018). Supercharging protein ions in native mass spectrometry using theta capillary nanoelectrospray ionization mass spectrometry and cyclic alkylcarbonates. *Analytica Chimica Acta*, *1003*, 1–9.
14. Miladinovic, S. M., Fornelli, L., Lu, Y., Piech, K. M., Girault, H. H., & Tsybin, Y. O. (2012). In-spray supercharging of peptides and proteins in electrospray ionization mass spectrometry. *Analytical Chemistry*, *84*, 4647–4651.
15. Yin, S., & Loo, J. A. (2011). Top-down mass spectrometry of supercharged native protein–ligand complexes. *International Journal of Mass Spectrometry*, *300*, 118–122.
16. Nshanian, M., Lakshmanan, R., Chen, H., Loo, R. R. O, & Loo, J. A. (2018). Enhancing sensitivity of liquid chromatography–mass spectrometry of peptides and proteins using supercharging agents. *International Journal of Mass Spectrometry*, *427*, 157–164.
17. Attygalle, A. B., Xia, H., & Pavlov, J. (2017). Influence of ionization source conditions on the gas-phase protomer distribution of anilinium and related cations. *Journal of the American Society for Mass Spectrometry*, *28*, 1575–1586.
18. Xia, H., & Attygalle, A. B. (2017). Untrapping kinetically trapped ions: The role of water vapor and ion-source activation conditions on the gas-phase protomer ratio of benzocaine revealed by ion-mobility mass spectrometry. *Journal of the American Society for Mass Spectrometry*, *28*, 2580–2587.
19. Xia, H., & Attygalle, A. B. (2018). Transformation of the gas-phase favored O-protomer of p-aminobenzoic acid to its unfavored N-protomer by ion activation in the presence of water vapor: An ion-mobility mass spectrometry study. *Journal of Mass Spectrometry: JMS*, *53*, 353–360.
20. Patrick, A. L., Cismesia, A. P., Tesler, L. F., & Polfer, N. C. (2017). Effects of ESI conditions on kinetic trapping of the solution-phase protonation isomer of p-aminobenzoic acid in the gas phase. *International Journal of Mass Spectrometry*, *418*, 148–155.
21. Cismesia, A. P., Nicholls, G. R., & Polfer, N. C. (2017). Amine vs. carboxylic acid protonation in ortho-, meta-, and para-aminobenzoic acid: An IRMPD spectroscopy study. *Journal of Molecular Spectroscopy*, *332*, 79–85.
22. Matthews, E., & Dessent, C. E. H. (2017). Experiment and theory confirm that UV laser photodissociation spectroscopy can distinguish protomers formed via electrospray. *Physical Chemistry Chemical Physics: PCCP*, *19*, 17434–17440.
23. Bull, J. N., Coughlan, N. J. A., & Bieske, E. J. (2017). Protomer-specific photochemistry investigated using ion mobility mass spectrometry. *The Journal of Physical Chemistry. A*, *121*, 6021–6027.

24. Lalli, P. M., Iglesias, B. A., Toma, H. E., Sa, G. F., Daroda, R. J., Silva Filho, J. C., Szulejko, J. E., Araki, K., & Eberlin, M. N. (2012). Protomers: Formation, separation and characterization via travelling wave ion mobility mass spectrometry. *Journal of Mass Spectrometry: JMS*, *47*, 712–719.
25. Wu, R. R., Hamlow, L. A., He, C. C., Nei, Y.-W., Berden, G., Oomens, J., & Rodgers, M. T. (2017). N3 and O2 protonated conformers of the cytosine mononucleotides coexist in the gas phase. *Journal of the American Society for Mass Spectrometry*, *28*, 1638–1646.
26. Langer, J., Günther, A., Seidenbecher, S., Berden, G., Oomens, J., & Dopfer, O. (2014). Probing protonation sites of isolated flavins using IR spectroscopy: From lumichrome to the cofactor flavin mononucleotide. *Chemphyschem: A European Journal of Chemical Physics and Physical Chemistry*, *15*, 2550–2562.
27. Warnke, S., Seo, J., Boschmans, J., Sobott, F., Scrivens, J. H., Bleiholder, C., Bowers, M. T., Gewinner, S., Schöllkopf, W., Pagel, K., & Von Helden, G. (2015). Protomers of benzocaine: solvent and permittivity dependence. *Journal of the American Chemical Society*, *137*, 4236–4242.
28. Marlton, S. J. P., Mckinnon, B. I., Ucur, B., Bezzina, J. P., Blanksby, S. J., & Trevitt, A. J. (2020). Discrimination between protonation isomers of quinazoline by ion mobility and UV-photodissociation action spectroscopy. *Journal of Physical Chemistry Letters*, *11*, 4226–4231.
29. Valadbeigi, Y., & Causon, T. (2023). Monitoring intramolecular proton transfer with ion mobility-mass spectrometry and in-source ion activation. *Chemical Communications*, (Cambridge, England), 1673–1676.
30. Mccann, A., Kune, C., Massonnet, P., Far, J., Ongena, M., Eppe, G., Quinton, L., & De Pauw, E. (2022). Cyclic peptide protomer detection in the gas phase: Impact on CCS measurement and fragmentation patterns. *Journal of the American Society for Mass Spectrometry*, *33*, 851–858.
31. Zhang, J. D, Donor, M. T., Rolland, A. D., Leeming, M. G., Wang, H., Trevitt, A. J., Kabir, K. M. M, Prell, J. S., & Donald, W. A. (2020). Protonation isomers of highly charged protein ions can be separated in FAIMS-MS. *International Journal of Mass Spectrometry*, *457*, 116425.
32. Lermyte, F., Theisen, A., & O'Connor, P. B. (2021). Solution condition-dependent formation of gas-phase protomers of alpha-synuclein in electrospray ionization. *Journal of the American Society for Mass Spectrometry*, *32*, 364–372.
33. Going, C. C., & Williams, E. R. (2015). Supercharging with m-nitrobenzyl alcohol and propylene carbonate: forming highly charged ions with extended, near-linear conformations. *Analytical Chemistry*, *87*, 3973–3980.
34. Donor, M. T., Ewing, S. A., Zenaidee, M. A., Donald, W. A., & Prell, J. S. (2017). Extended protein ions are formed by the chain ejection model in chemical supercharging electrospray ionization. *Analytical Chemistry*, *89*, 5107–5114.
35. Iavarone, A. T., & Williams, E. R. (2003). Mechanism of charging and supercharging molecules in electrospray ionization. *Journal of the American Chemical Society*, *125*, 2319–2327.
36. Ogorzalek Loo, R. R., Lakshmanan, R., & Loo, J. A. (2014). What protein charging (and supercharging) reveal about the mechanism of electrospray ionization. *Journal of the American Society for Mass Spectrometry*, *25*, 1675–1693.
37. Sterling, H. J., Prell, J. S., Cassou, C. A., & Williams, E. R. (2011). Protein conformation and supercharging with DMSO from aqueous solution. *Journal of the American Society for Mass Spectrometry*, *22*, 1178–1186.
38. Wysocki, V. H., Tsaprailis, G., Smith, L. L., & Breci, L. A. (2000). Mobile and localized protons: a framework for understanding peptide dissociation. *Journal of Mass Spectrometry*, *35*, 1399–1406.
39. Dongré, A. R., Jones, J. L., Somogyi, Á., & Wysocki, V. H. (1996). Influence of peptide composition, gas-phase basicity, and chemical modification on fragmentation efficiency: Evidence for the mobile proton model. *Journal of the American Chemical Society*, *118*, 8365–8374.
40. Paizs, B., & Suhai, S. (2006). Fragmentation pathways of protonated peptides. *ChemInform*, *37*, doi:10.1002/mas.20024
41. Tsaprailis, G., Nair, H., Somogyi, Á., Wysocki, V. H., Zhong, W., Futrell, J. H., Summerfield, S. G., & Gaskell, S. J. (1999). Influence of secondary structure on the fragmentation of protonated peptides. *Journal of the American Chemical Society*, *121*, 5142–5154.
42. Wang, H., Leeming, M. G., Ho, J., & Donald, W. A. (2019). Origin and prediction of highly specific bond cleavage sites in the thermal activation of intact protein ions. *Chemistry (Weinheim An Der Bergstrasse, Germany)*, *25*, 823–834.
43. Schnier, P. D., Gross, D. S., & Williams, E. R. (1995). On the maximum charge state and proton transfer reactivity of peptide and protein ions formed by electrospray ionization. *Journal of the American Society for Mass Spectrometry*, *6*, 1086–1097.
44. Morrison, L. J., & Brodbelt, J. S. (2016). Charge site assignment in native proteins by ultraviolet photodissociation (UVPD) mass spectrometry. *Analyst*, *141*, 166–176.
45. Bashyal, A., Sanders, J. D., Holden, D. D., & Brodbelt, J. S. (2019). Top-down analysis of proteins in low charge states. *Journal of the American Society for Mass Spectrometry*, *30*, 704–717.
46. Bush, M. F., Hall, Z., Giles, K., Hoyes, J., Robinson, C. V., & Ruotolo, B. T. (2010). Collision cross sections of proteins and their complexes: a calibration framework and database for gas-phase structural biology. *Analytical Chemistry*, *82*, 9557–9565.
47. Ruotolo, B. T., Benesch, J. L. P., Sandercock, A. M., Hyung, S.-J., & Robinson, C. V. (2008). Ion mobility–mass spectrometry analysis of large protein complexes. *Nature Protocols*, *3*, 1139–1152.
48. Cai, W., Guner, H., Gregorich, Z. R., Chen, A. J., Ayaz-Guner, S., Peng, Y., Valeja, S. G., Liu, X., & Ge, Y. (2016). MASH Suite Pro: A Comprehensive Software Tool for Top-Down Proteomics. *Molecular & Cellular Proteomics: MCP*, *15*, 703–714.
49. Guner, H., Close, P. L., Cai, W., Zhang, H., Peng, Y., Gregorich, Z. R., & Ge, Y. (2014). MASH Suite: A user-friendly and versatile software interface for high-resolution mass spectrometry data interpretation and visualization. *Journal of the American Society for Mass Spectrometry*, *25*, 464–470.
50. Wu, Z., Roberts, D. S., Melby, J. A., Wenger, K., Wetzel, M., Gu, Y., Ramanathan, S. G., Bayne, E. F., Liu, X., Sun, R., Ong, I. M., Mcilwain, S. J., & Ge, Y. (2020). MASH Explorer: A Universal Software Environment for Top-Down Proteomics. *Journal of Proteome Research*, *19*, 3867–3876.
51. Mcilwain, S. J., Wu, Z., Wetzel, M., Belongia, D., Jin, Y., Wenger, K., Ong, I. M., & Ge, Y. (2020). Enhancing top-down proteomics data analysis by combining deconvolution results through a machine learning strategy. *Journal of the American Society for Mass Spectrometry*, *31*, 1104–1113.
52. Kaur, P., & O'Connor, P. B. (2006). Algorithms for automatic interpretation of high resolution mass spectra. *Journal of the American Society for Mass Spectrometry*, *17*, 459–468.
53. Konermann, L., Ahadi, E., Rodriguez, A. D., & Vahidi, S. (2013). Unraveling the mechanism of electrospray ionization. *Analytical Chemistry*, *85*, 2–9.
54. Li, J., Santambrogio, C., Brocca, S., Rossetti, G., Carloni, P., & Grandori, R. (2016). Conformational effects in protein electrospray-ionization mass spectrometry. *Mass Spectrometry Reviews*, *35*, 111–122.
55. Schaffer, L. V., Millikin, R. J., Miller, R. M., Anderson, L. C., Fellers, R. T., Ge, Y., Kelleher, N. L., Leduc, R. D., Liu, X., Payne, S. H., Sun, L., Thomas, P. M., Tucholski, T., Wang, Z., Wu, S., Wu, Z., Yu, D., Shortreed, M. R., & Smith, L. M. (2019). Identification and quantification of proteoforms by mass spectrometry. *Proteomics*, *19*, 1800361.
56. Holt, M. V., Wang, T., & Young, N. L. (2019). High-throughput quantitative top-down proteomics: Histone H4. *Journal of the American Society for Mass Spectrometry*, *30*, 2548–2560.
57. Cupp-Sutton, K. A., & Wu, S. (2020). High-throughput quantitative top-down proteomics. *Molecular Omics*, *16*, 91–99.
58. Harrison, A. G., & Yalcin, T. (1997). Proton mobility in protonated amino acids and peptides. *International Journal of Mass Spectrometry and Ion Processes*, *165–166*, 339–347.

59. Johnson, R. S., Krylov, D., & Walsh, K. A. (1995). Proton mobility within electrosprayed peptide ions. *Journal of Mass Spectrometry*, *30*, 386–387.
60. Burlet, O., Orkiszewski, R. S., Ballard, K. D., Gaskell, S. J., & Bertrand, M. J. (1992). Charge promotion of low-energy fragmentations of peptide ions. *Rapid Communications in Mass Spectrometry: RCM*, *6*, 658–662.
61. Xie, Y., Zhang, J., Yin, S., & Loo, J. A. (2006). Top-down ESI-ECD-FT-ICR mass spectrometry localizes noncovalent protein-ligand binding sites. *Journal of the American Chemical Society*, *128*, 14432–14433.
62. Phillips, A. S., Gomes, A. F., Kalapothakis, J. M. D., Gillam, J. E., Gasparavicius, J., Gozzo, F. C., Kunath, T., Macphee, C., & Barran, P. E. (2015). Conformational dynamics of α-synuclein: insights from mass spectrometry. *Analyst*, *140*, 3070–3081.
63. Wongkongkathep, P., Han, J. Y., Choi, T. S., Yin, S., Kim, H. I., & Loo, J. A. (2018). Native top-down mass spectrometry and ion mobility MS for characterizing the cobalt and manganese metal binding of α-synuclein protein. *Journal of the American Society for Mass Spectrometry*, *29*, 1870–1880.
64. Lermyte, F., Everett, J., Brooks, J., Bellingeri, F., Billimoria, K., Sadler, P. J., O'Connor, P. B., Telling, N. D., & Collingwood, J. F. (2019). Emerging approaches to investigate the influence of transition metals in the proteinopathies. *Cells*, *8*, 1231.
65. Good, D. M., Wirtala, M., McAlister, G. C., & Coon, J. J. (2007). Performance characteristics of electron transfer dissociation mass spectrometry. *Molecular & Cellular Proteomics: MCP*, *6*, 1942–1951.
66. Pitteri, S. J., & Mcluckey, S. A. (2005). Recent developments in the ion/ion chemistry of high-mass multiply charged ions. *Mass Spectrometry Reviews*, *24*, 931–958.
67. Hamdy, O. M., & Julian, R. R. (2012). Reflections on charge state distributions, protein structure, and the mystical mechanism of electrospray ionization. *Journal of the American Society for Mass Spectrometry*, *23*, 1–6.
68. Perez-Riverol, Y., Bai, J., Bandla, C., García-Seisdedos, D., Hewapathirana, S., Kamatchinathan, S., Kundu, D. J., Prakash, A., Frericks-Zipper, A., Eisenacher, M., Walzer, M., Wang, S., Brazma, A., & Vizcaíno, J. A. (2022). The PRIDE database resources in 2022: A hub for mass spectrometry-based proteomics evidences. *Nucleic Acids Research*, *50*, D543–D552.
69. Deutsch, E. W., Bandeira, N., Sharma, V., Perez-Riverol, Y., Carver, J. J., Kundu, D. J., García-Seisdedos, D., Jarnuczak, A. F., Hewapathirana, S., & Pullman, B. S. et al. (2020). The ProteomeXchange consortium in 2020: Enabling 'big data' approaches in proteomics. *Nucleic Acids Research*, *48*, D1145–D1152.

SUPPORTING INFORMATION

Additional supporting information may be found online https://doi.org/10.1002/pmic.202300082 in the Supporting Information section at the end of the article.

How to cite this article: Habeck, T., Maciel, E. V. S., Kretschmer, K., & Lermyte, F. (2024). Charge site manipulation to enhance top-down fragmentation efficiency. *Proteomics*, *24*, e2300082. https://doi.org/10.1002/pmic.202300082